Numerical and Theoretical Investigation of the Acoustoelastic Effect of Tensile and Shear Stress on the Propagation of Ultrasonic Lamb Waves in Plate

ALAN C. KUBRUSLY, CHRISTOS V. STAMOPOULOS, SHOROB ALAM BHUIYAN, LUIS PAULO BRASIL DE SOUZA, PEIYUAN ZHOU and FOTIS KOPSAFTOPOULOS

ABSTRACT

Initial stress affects the propagation of ultrasonic guided waves and therefore is relevant for the structural health monitoring field. Typically, only normal pre-stress is considered in the wave propagation. In this work, the effect of another relevant loading case, namely, shear stress, on the propagation of ultrasonic guided waves is investigated utilizing the finite element and semi-analytical finite element modeling while a stochastic metamodeling analysis is also presented. An aluminum plate is considered where the initial stress is set either as longitudinal tensile or shear stress along the propagating direction. Both methods show good agreement, revealing that for the fundamental Lamb wave modes and evaluated stress levels, the phase speed difference due to shear stress is less than due to tensile stress; however, speed changes quadratically with the shear stress level, unlike tensile stress which shows a linear behavior. Additionally, autoregressive and functional stochastic models are employed in view of a metamodeling approach to represent and assess stress effects on guided waves.

INTRODUCTION

Assessing the physical integrity of structures is vital in many sectors, such as within the aerospace, energy, and environmental communities [1]. In the structural health monitoring (SHM) context, ultrasonic guided waves (UGW) play an important role. According to Yang et al. [2], the main advantages of UGW for SHM are (i) their ability to propagate long distances, allowing large areas to be monitored; (ii) fast inspection and monitoring capabilities; (iii) high sensitivity to defects, including internal ones; and (iv) relatively low cost and low-energy consumption.

UGWs propagate in structures where the thickness dimension is in the order of, or smaller than, the wavelength of the wave in the medium, which then plays the role of a waveguide. The direction of propagation follows the longitudinal, or axial, dimension of the waveguide, while it presents a characteristic wavefield profile across the thickness

Alan C Kubrusly, Email: alan@cpti.cetuc.puc-rio.br. Department of Electrical Engineering, Pontifical Catholic University of Rio de Janeiro, Rio de Janeiro, Brazil; Intelligent Structural Systems Lab (ISSL), Department of Mechanical, Aerospace and Nuclear Engineering, Rensselaer Polytechnic Institute, Troy, NY, USA

dimension, which is known as a guided wave mode. Each guided wave mode propagates at a particular speed and, generally, they are dispersive, meaning that its propagation speed depends on the frequency [3].

Stress assessment is vital in structures that are subject to high load conditions. As per the acoustoelastic theory [4], the propagation speed of ultrasonic waves depends on the stress state of the medium in which they propagate. In order to analyze the stress dependence of UGW one can resort to analytical [5, 6], semi-analytical [7, 8] or numerical methods [9, 10]. The initial stress effect on UGW is complex: each UGW mode shows a different dependence on stress, which also changes with frequency [5, 6]. Usually, only tensile or biaxial tensile pre-stress is considered [5, 6, 9, 10]. For instance, functional series time-varying autoregressive models [11] were applied to damage detection employing UGW in plates under varied loading conditions, and Gaussian process Automatic regression models [12] were applied in order to predict the structural state, which consisted of both varying damage and tensile load conditions. Analysis of the shear stress effect on the propagation characteristics of UGW has received little attention [8], despite also being a common load state in practical scenarios.

This work theoretically and numerically investigates the effect of shear stress, in addition to tensile stress, on the propagation of ultrasonic Lamb waves in plates aiming at SHM applications. Additionally, parametric time-series statistical modeling was applied to UGW time-domain signals to evaluate the influence of tensile and shear stress on the model parameters across multiple stress levels.

EFFECT OF INITIAL STRESS ON ULTRASONIC GUIDED WAVES

Acoustoelasticity studies the variation of the acoustic wave speed in bodies subject to an initial stress state. It consists of non-linear relationships between stress and strain that rule the dynamic response superimposed to the initial pre-deformation. The theory of weakly non-linear elasticity considers the strain energy function expanded, typically, up to third-order terms. It is employed to describe the acoustoelastic effect in stiff solids, as metals, with small pre-stress [4].

Three frames of reference are required in order to derive the acoustoelastic theory of motion. A body is deformed from its natural (undeformed) state ($\xi_\alpha, \alpha = 1, 2, 3$) to a statically deformed state, called initial state ($X_I, I = 1, 2, 3$). Wave motion is superimposed on the initial state, leading to the final state ($x_i, i = 1, 2, 3$). The initial displacement ($\boldsymbol{u}^i = \boldsymbol{X} - \boldsymbol{\xi}$) takes the body from the natural to the initial configuration, whereas the incremental displacement ($\boldsymbol{u} = \boldsymbol{X} - \boldsymbol{x}$) takes the body from the initial to the final, dynamic, state. Within the weakly non-linear acoustoelastic theory, the body is considered hyperelastic and both the fourth- and sixth-order elastic tensors are employed to describe the relationship between natural and final states. For an isotropic material, the fourth-order elastic tensor, $C_{\alpha\beta\lambda\delta}$, depends on the usual elastic moduli, such as the Lamé constants, namely λ and μ, and the sixth-order elastic tensor, $C_{\alpha\beta\lambda\delta\zeta\eta}$, depends on third-order moduli, such as the Murnaghan constants, namely, l, m and n. Their expressions are reported elsewhere [4].

From the equation of motion, considering the initial and incremental stress, as well as the initial and incremental displacement gradient, with several manipulations [6], includ-

ing neglecting second-order incremental entities, one reaches a typical wave equation:

$$A_{\alpha\beta\gamma\delta}\frac{\partial^2 u_\gamma}{\partial\xi_\beta\partial\xi_\delta} = \rho^0\frac{\partial^2 u_\alpha}{\partial t^2} \quad . \tag{1}$$

where ρ^0 is the natural mass density and tensor $\boldsymbol{A}$ is given by [6]

$$A_{\alpha\beta\gamma\delta} = s^i_{\beta\delta}\,\delta_{\alpha\gamma} + C_{\alpha\beta\gamma\delta} + C_{\alpha\beta\lambda\delta}\frac{\partial u^i_\gamma}{\partial\xi_\lambda} + C_{\lambda\beta\gamma\delta}\frac{\partial u^i_\alpha}{\partial\xi_\lambda} + C_{\alpha\beta\lambda\delta\zeta\eta}\,\varepsilon^i_{\zeta\eta} \quad , \tag{2}$$

such that $\varepsilon^i_{\alpha\beta}$ is the initial strain, given by the symmetric part of the initial displacement gradient, $\partial u^i_\alpha/\partial\xi_\beta$. Summation over repeated index is assumed. Assuming small initial stress, the usual Hooke's law can be used to relate initial stress and initial strain, namely, $s^i_{\alpha\beta} = C_{\alpha\beta\gamma\delta}\,\varepsilon^i_{\gamma\delta}$.

By solving the wave equation, Eq.(1), one can obtain the wave speed for the UGW under initial stress. This can be performed by resorting to common methods for UGW analysis, such as the partial wave technique [5, 6], or the semi-analytical finite element (SAFE) method [7, 8]. The latter is used herein.

SEMI-ANALYTICAL FINITE ELEMENT SOLUTION FOR ACOUSTOELASTIC GUIDED WAVES

The SAFE method consists of employing the Finite Element approach to the waveguide cross-section, whilst considering a harmonic wave motion along the waveguide longitudinal direction [13], being a handy technique for UGW analysis. The SAFE approach can be extended to acoustoelastic waveguides, as proposed in [7]; its main steps are summarized below.

The waveguide cross-section, which lies in the ξ_2-ξ_3 plane, is discretized in n_e elements in which the displacement field, given by a harmonic propagation in the ξ_1 direction, is given by $\boldsymbol{u} = \boldsymbol{N}\,\boldsymbol{u}^e\,e^{i(\kappa\xi_1-\omega t)}$, where κ is the wavenumber, ω the angular frequency and $i=\sqrt{-1}$; $\boldsymbol{u}^e$ is the nodal displacement field, and $\boldsymbol{N}$ is the shape function matrix. Considering the weak integral form for the wave equation, Eq.(1), and boundary conditions of free incremental stress, with the displacement field given as above, and after several manipulations [7], one obtains an eigenvalue problem:

$$\left[\boldsymbol{K}_1 - \boldsymbol{K}_4 + i\kappa(\boldsymbol{K}_2 - \boldsymbol{K}_5) + \kappa^2\boldsymbol{K}_3 - \omega^2\boldsymbol{M}\right]\boldsymbol{U} = 0 \tag{3}$$

where $\boldsymbol{U}$ is the global displacement amplitude vector, along all the waveguide elements, and the matrices $\boldsymbol{K}_1$ to $\boldsymbol{K}_5$ and $\boldsymbol{M}$ are assembled from the respective individual element matrices, whose expressions can de found in [7]. For each frequency ω, Eq.3 is solved in order to obtain the wavenumber, κ, for the possible guided wave modes within the waveguide. Therefore, phase speed can be calculated by $c = \omega/\kappa$.

The waveguide considered here consists of a flat plate oriented as shown in Fig. 1(a). Therefore, it constitutes a two-dimensional problem, in which the cross-section is one-dimension, along the ξ_2-direction. The SAFE method was employed to analyze the stress effect on UGW propagating in an aluminum plate whose constants are reported in Table I. Two initial-stress cases are considered, namely, longitudinal tensile stress

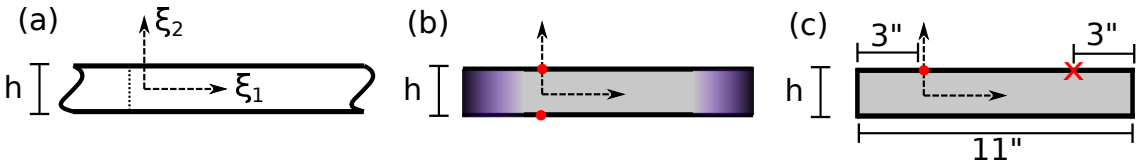

Figure 1. Plate geometry and coordinate system. SAFE approach (a) where the plate is discretized in the cross-section only; FEM modeled plate with absorber at the plate's end to mimic an infinitely long plate (b) and finite long plate (c). Red dots and cross stand for generation and reception points, respectively.

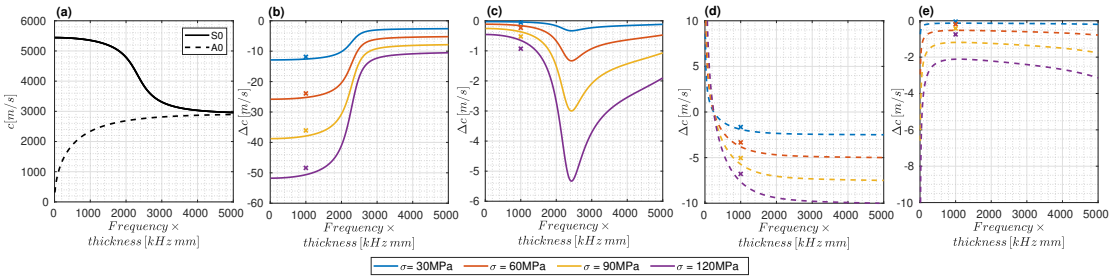

Figure 2. Phase speed dispersion curves under longitudinal tensile and shear stresses, calculated with the SAFE method, for the S0 (continuous line) and A0 (dashed line) guided wave modes. Dispersion curves without pre-stress (a); phase speed difference relative to the zero stress case for the S0 mode under longitudinal tensile stress (b) and shear stress (c), and for the A0 mode under longitudinal tensile stress (d) and shear stress (e). Crosses represent the obtained values with time-domain FEM simulation.

parallel to the propagation direction, and shear stress parallel to the propagation direction. Simple shear is considered for the latter; that is, the initial displacement is given by $u_1^i = (\tau/\mu)\xi_2$, where τ is the shear stress magnitude.

TABLE I. Aluminum constants [14].

ρ kg/m^3	λ GPa	μ GPa	l GPa	m GPa	n GPa
2700	54.9	26.5	-252.2	-324.9	-351.2

Fig. 2(a) shows the computed phase speed dispersion curves for the A0 and S0 Lamb wave modes without pre-stress, c_0, and Fig. 2(b-e) show the phase speed difference relative to the null stress case, namely, $\Delta c = c_\sigma - c_0$, where c_σ is the phase speed under stress. Fig. 2(b-c) show for the S0 wave mode under tensile and shear stresses, respectively, and Fig. 2(d-e) show for the A0 wave mode under tensile and shear stresses, respectively. The tensile stress case, Fig. 2(b) and (d), shows good agreement with previously reported results elsewhere [5], with higher speed change for the S0 wave mode at low frequency and a sign change on Δc for the A0 mode at a few hundred kHz mm. As can be seen in Fig. 2(c) and (e), shear stress impose a lower speed difference than tensile stress does. Moreover, unlike the tensile stress case, where Δc shows a linear trend with the increasing stress level, for the shear stress one can observe a non-linear trend of with increasing stress level. This phenomenon is further analyzed in the next section.

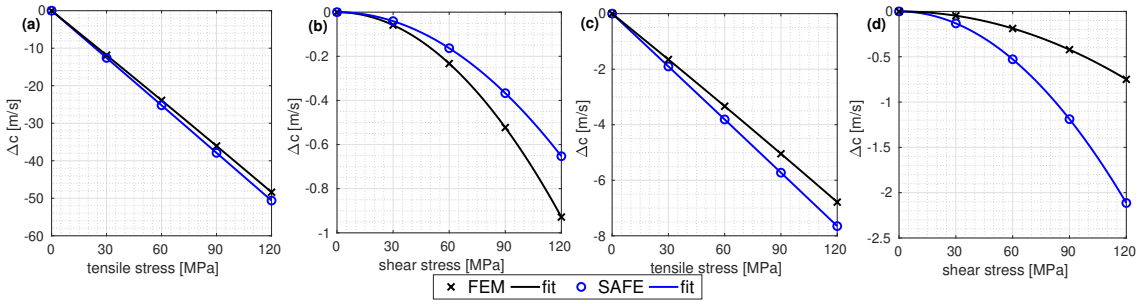

Figure 3. Phase speed difference, relative to the unstressed state, for S0 (a-b) and A0 (c-d) wave modes in a 10 mm-thick aluminum plate at 100 kHz, obtained with SAFE (blue circles) and FEM (black crosses) methods for shear (b and d) and tensile pre-stress (a and c).

FINITE ELEMENT SIMULATION OF ACOUSTOELASTIC GUIDED WAVES

In order to investigate the initial stress effect directly on the received ultrasonic signals, one can resort to finite element simulations [9,10]. The acoustoelastic effect can be simulated by setting the material as hyperelastic under the Murnaghan model, followed by a two-step simulation procedure. The first step consists of imposing the load condition, and on the second step, the usual time-transient solution for the wave propagation over the initially stressed body is performed [9, 10].

A two-dimensional model of a 10 mm-thick aluminum plate, whose materials constants are given by Table I, was used, where either a longitudinal tensile or shear stress was imposed. The former was applied as a normal loading to the plate's end, and the latter consisted of tangential loading to the plate's surface, both in the ξ_1 direction. The dynamic motion was imposed by applying point forces at both plate's surfaces modulated by a 5-cycle tone burst signal at 100 kHz. Both fundamental Lamb wave modes, namely, A0 and S0 modes were independently generated. In order to generate the A0 modes, symmetric normal forces were imposed at both surfaces, whilst the S0 mode was generated by imposing symmetric tangential forces. In order to mimic an infinite-long medium, absorbers were applied to both plate's ends. Fig. 1(b) depicts the plate's model.

From the received signals, the phase speed was calculated and compared to theoretical predictions computed with the SAFE method. Fig. 2 reports the FEM calculated phase speed under stress as crosses superposed to the theoretical dispersion curves calculated with the SAFE method. As can be seen, good agreement was obtained for both wave modes under tensile and shear stresses, mainly for the S0 wave mode. Fig. 3 shows the phase speed as a function of the stress level computed both with FEM or SAFE methods. Despite the dependence on the stress level for shear pre-stress being lower than for tensile pre-stress, it is clear in Fig. 3 that the wave speed does not behave linearly with the stress level, like with tensile stress. As shown by the trend lines, both numerical and theoretical indicate that the speed changes quadratically with the shear stress level, whilst linearly with the tensile stress.

PARAMETRIC MODELING OF UGW SIGNAL UNDER MULTIPLE STRESS LEVELS

The effects of multiple stress levels on the simulated UGW signals were further investigated through parametric time-series statistical modeling. Specifically, two parametric models are employed: a standard AutoRegressive (AR) model for preliminary analysis of tensile and shear stress influence, and an advanced Functionally Pooled AutoRegressive (FP–AR) model to capture parameter evolution over a continuous stress range.

Both models can be expressed through a generalized AR framework:

$$y_k[t] + \sum_{i=1}^{n} a_i(k) \cdot y_k[t-i] = e_k[t], \qquad e_k[t] \sim \mathcal{N}(0, \sigma_e^2(k)) \quad . \tag{4}$$

In the AR case, the stress level k is fixed, yielding constant coefficients $a_i(k) = a_i$ and residuals $e_k[t] = e[t]$, resulting in the classical AR model [15]. AR model identification follows standard procedures, including Ordinary Least Squares (OLS) estimation, BIC-based order selection, and residual whiteness testing [15, 16].

In the FP–AR model, the coefficients $a_i(k)$ are modeled as explicit functions of the stress level k using a p-dimensional functional subspace:

$$a_i(k) = \sum_{j=1}^{p} a_{i,j} \cdot G_j(k) \quad . \tag{5}$$

Here, $G_j(k)$ are mutually independent basis functions (e.g., Chebyshev polynomials), and $a_{i,j}$ are the associated projection coefficients. Model identification involves selecting the AR order n and subspace dimensionality p via BIC minimization, validating residual whiteness, and estimating parameters using OLS with data pooling [17]. This formulation enables effective modeling of parameter variability over the continuous stress domain.

PARAMETRIC MODELING RESULTS

Aiming at a scenario of more practical interest for the parametric time-series statistical analysis, a new set of simulations was performed on a 2.36 mm-thick, 11 in-long aluminum plate without absorbers at the end, therefore allowing reflections. Excitation consisted of a normal force applied to a single surface of the plate, at 3 in from the left end, which was modulated by a 5-cycle tone burst signal at 100 kHz. Received signals were acquired at 3 in from the right end, as illustrated in Fig. 1(c). The same material constants (Table I) were used. The stress level was varied from 0 to 200 MPa in 10 MPa steps for both tensile and shear stress loading. Fig. 4 shows the received signals for tensile stress.

Based on the 21 received UGW signals covering the range of [0, 200] MPa tensile or shear stress, with a 10 MPa step, a total of 42 conventional AR(6) models are obtained. Each model has six estimated parameters (model order $n = 6$), with an average of 687.67 samples per parameter. The AR models yield a condition number of 9.97×10^9 and a

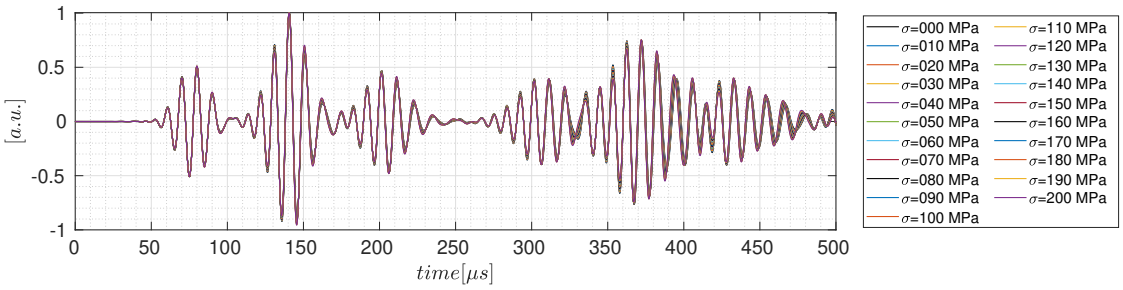

Figure 4. FEM simulation of UGW received signal in an 11 in-long, 2.36 mm thick aluminum plate under longitudinal tensile stress up to 200 MPa.

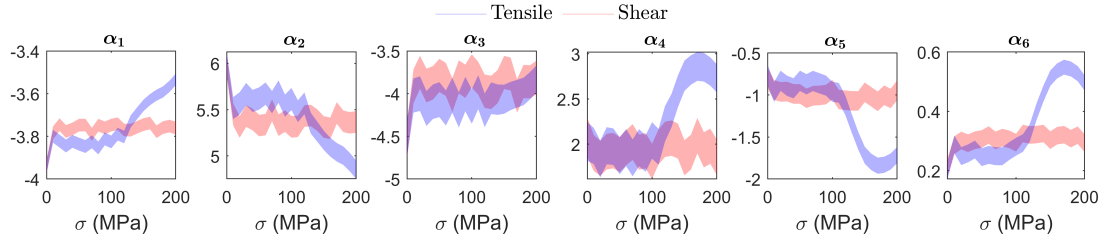

Figure 5. AR(6) model parameters versus stress levels: The shaded regions show ± 3 standard deviation around the parameter mean. Tensile-stress cases are shaded in blue, whereas shear-stress cases are shaded in red. Note that shear stress effects on the model parameters are significantly less pronounced compared to the normal stress.

Bayesian Information Criterion (BIC) value of -44.44. Fig. 5 shows the six parameters of all AR models, $a_1, a_2, \ldots, a_6$, as functions of the stress level (σ, MPa). Specifically, each subplot presents a single parameter across all AR models, corresponding to the various stresses considered. The shaded regions indicate the ± 3 standard deviation around the mean parameter values, with tensile stress cases shaded in blue and shear stress cases shaded in red. As can be seen, the effects of shear stress on the model parameters are significantly less pronounced compared to tensile stress, across all six parameters, except for a_3, where both tensile and shear stress induce only minor variability.

Based on the above, it is evident that further parametric modeling of the received GW signals as a function of shear stress level would provide little additional value. Therefore, only the 21 received GW signals corresponding to tensile stress levels in the range of [0, 200] MPa, with a 10 MPa step, are now utilized for the identification of an FP–AR$(6)_5$ model with order $n = 6$ and a functional subspace comprising $p = 5$ sequential Chebyshev polynomials. This model represents the GW signals across the continuous tensile stress range of [0, 200] MPa. The FP–AR$(6)_5$ model is estimated using 52.78 samples per parameter, yielding a condition number of 4.08×10^{12} and a significantly lower Bayesian Information Criterion (BIC) value of -908.21. Fig. 6 illustrates the six parameters of the FP–AR$(6)_5$ model as continuous functions of tensile stress within the considered range [0, 200] MPa. Specifically, each subplot presents a single parameter of the FP–AR$(6)_5$ model as a function of the tensile stress level. The blue shaded regions indicate the ± 2 standard deviation around the mean parameter value. As can be observed, the FP-AR model not only effectively captures the variability in the model parameters induced by different tensile stress levels, but also provides an accurate repre-

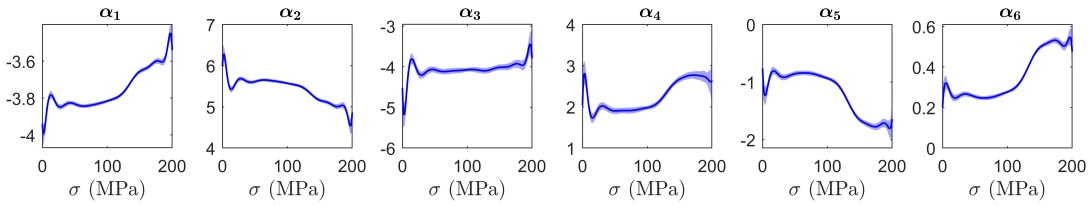

Figure 6. FP–AR$(6)_5$ model parameters versus tensile stress levels: The shaded region shows ± 2 standard deviations around the parameter mean.

sentation of the parameters at any stress level within the considered range. Additionally, it is noted that the parameters exhibit greater variability at the low and high ends of the stress range, specifically below 15 MPa and above 100 MPa, while maintaining a relatively constant value in the middle range.

Furthermore, Fig. 7(a) illustrates the relationship between the first (a_1) and the last (a_6) parameter of the FP–AR$(6)_5$ model as a function of the tensile stress level, while Fig. 7(b) extends this analysis to include the second parameter (a_2) alongside a_1 and a_6. In both figures, the tensile stress level is represented through a color gradient, providing a clear visualization of the continuous dependency of the model parameters on the stress level. In Fig. 7(b), 1000 realizations of the estimated model parameters are presented, offering a more comprehensive assessment of the model's behavior under varying stress conditions. The trajectories of the parameters indicate a well-defined, continuous relationship across the tensile stress range, with only minor dispersion around the mean trajectories. This suggests that the FP–AR$(6)_5$ model is not only capable of capturing the primary dependencies among the parameters but also effectively represents the inherent variability induced by the different stress levels. Moreover, the clustering of trajectories in the mid-range stress levels, combined with the increased spread at the lower and higher ends, is consistent with the earlier observation of higher parameter variability near the extremes of the tensile stress range (below 15 MPa and above 100 MPa). This indicates that the model is particularly sensitive to changes in the stress state at these critical levels, reflecting potential threshold phenomena that are not as pronounced in

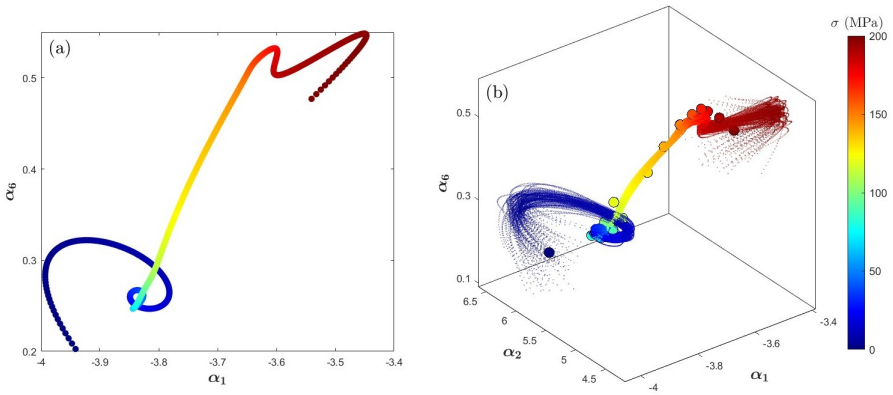

Figure 7. FP–AR$(6)_5$ parameter trajectories at tensile stress levels from 0 to 200 MPa (see colour bar). (a) Evolution of parameters a_1 and a_6; (b) Evolution of parameters a_1, a_2, and a_6. The large dots correspond to the parameters of the AR(6) model.

the mid-stress region.

The FP–AR$(6)_5$ model effectively represents the received UGW signals across the different tensile stress levels, capturing both the continuous evolution of the model parameters and their inherent variability. This demonstrates the model's capability to adapt to stress-induced changes in wave propagation, making it promising for applications in real-time structural health monitoring. The observed stability of parameter trajectories in the mid-stress range, combined with increased variability near the low and high extremes, suggests that the model can effectively capture critical transitions in material behavior, potentially supporting early damage detection and residual life estimation. The same modeling approach can similarly be applied to shear stress, depending on the stress of interest.

CONCLUSION

The effect of initial tensile and shear stress on the propagation of UGW was investigated through the SAFE and FEM methods. The A0 and S0 Lamb wave modes in aluminum plate were analyzed and good agreement was obtained between the computed phase speed obtained with both methods. It has been observed, for the fundamental Lamb wave modes and evaluated stress levels herein, that the phase speed difference due to shear stress is roughly one order of magnitude less than due to tensile stress, however, speed changes quadratically with the shear stress level, unlike tensile stress which shows a linear behavior. A further investigation of the received UGW signals in a finite-long plate was performed resorting to time series analyses, employing AR and FP-AR models. Both showed agreement in capturing tensile stress sensitivity, particularly for stress levels below 15 MPa and above 100 MPa, where model parameter variability appears more pronounced. The AR model exhibits consistent behavior across shear stress levels, supporting the expectation that shear has a lower effect on the structure, which is primarily subjected to axial excitation. Thus, a single FP-AR model for tensile stress is adopted to accurately capture the continuous variation and intrinsic uncertainty of the parameters, highlighting its effectiveness in modeling stress-induced changes in guided wave propagation.

ACKNOWLEDGMENT

This work was supported in part by the Coordenação de Aperfeiçoamento de Pessoal de Nível Superior–Brasil (CAPES)–Finance Code 001, in part by the Carlos Chagas Filho Foundation for Research Support of Rio de Janeiro State (FAPERJ) under Processo SEI 260003/000549/2023, and in part by the Brazilian National Council for Scientific and Technological Development (CNPq).

REFERENCES

1. Frangopol, D. M. and K. Maute. 2003. "Life-cycle reliability-based optimization of civil and aerospace structures," *Computers & Structures*, 81(7):397–410, ISSN 0045-7949, doi: https://doi.org/10.1016/S0045-7949(03)00020-8.

2. Yang, Z., H. Yang, T. Tian, D. Deng, M. Hu, J. Ma, D. Gao, J. Zhang, S. Ma, L. Yang, H. Xu, and Z. Wu. 2023. "A review on guided-ultrasonic-wave-based structural health monitoring: From fundamental theory to machine learning techniques," *Ultrasonics*, 133:107014, ISSN 0041-624X, doi:https://doi.org/10.1016/j.ultras.2023.107014.
3. Rose, J. L. 2014. *Ultrasonic Guided waves in solid media*, Cambridge University Press.
4. Norris, A. N. 2024. *Finite-Amplitude Waves in Solids*, Springer Nature Switzerland, Cham, chap. 9, ISBN 978-3-031-58963-8, pp. 259–273, doi:"10.1007/978-3-031-58963-8".
5. Gandhi, N., J. E. Michaels, and S. J. Lee. 2012. "Acoustoelastic Lamb wave propagation in biaxially stressed plates," *The Journal of the Acoustical Society of America*, 132(3):1284–1293, doi:http://dx.doi.org/10.1121/1.4740491.
6. Kubrusly, A. C., A. M. B. Braga, and J. P. von der Weid. 2016. "Derivation of acoustoelastic Lamb wave dispersion curves in anisotropic plates at the initial and natural frames of reference," *The Journal of the Acoustical Society of America*, 140(4):2412–2417, ISSN 0001-4966, doi:10.1121/1.4964343.
7. Peddeti, K. and S. Santhanam. 2018. "Dispersion curves for Lamb wave propagation in prestressed plates using a semi-analytical finite element analysis," *The Journal of the Acoustical Society of America*, 143(2):829–840, ISSN 0001-4966, doi:10.1121/1.5023335.
8. Zuo, P., X. Yu, and Z. Fan. 2020. "Acoustoelastic guided waves in waveguides with arbitrary prestress," *Journal of Sound and Vibration*, 469:115113, ISSN 0022-460X, doi:https://doi.org/10.1016/j.jsv.2019.115113.
9. Yang, Y., C. T. Ng, M. Mohabuth, and A. Kotousov. 2019. "Finite element prediction of acoustoelastic effect associated with Lamb wave propagation in pre-stressed plates," *Smart Materials and Structures*, 28(9):095007, doi:10.1088/1361-665X/ab2dd3.
10. Qiu, L., X. Yan, X. Lin, and S. Yuan. 2019. "Multiphysics simulation method of lamb wave propagation with piezoelectric transducers under load condition," *Chinese Journal of Aeronautics*, 32(5):1071–1086, ISSN 1000-9361, doi:https://doi.org/10.1016/j.cja.2019.02.007.
11. Ahmed, S. and F. Kopsaftopoulos. 2022. "Statistical Active-Sensing Structural Health Monitoring via Stochastic Time-Varying Time Series Models," in *2022 American Control Conference (ACC)*, pp. 3599–3606, doi:10.23919/ACC53348.2022.9867472.
12. Amer, A. and F. Kopsaftopoulos. 2023. "Gaussian process regression for active sensing probabilistic structural health monitoring: experimental assessment across multiple damage and loading scenarios," *Structural Health Monitoring*, 22(2):1105–1139, doi:10.1177/14759217221098715.
13. Viola, E., A. Marzani, and I. Bartoli. 2007. *Semi-analytical Formulation for Guided Wave Propagationt*, Springer Vienna, Vienna, pp. 105–121, doi:10.1007/978-3-211-70963-4.
14. Stobbe, D. M. 2005. *Acoustoelasticity in 7075-T651 Aluminum and Dependence of Third Order Elastic Constants on Fatigue Damage*, Master's thesis, School of Mechanical Engineering, Georgia Institute of Technology.
15. Ljung, L. 1999. *System Identification: Theory for the User*, Prentice–Hall, 2nd edn.
16. Fassois, S. D. 2001. "Parametric Identification of Vibrating Structures," in S. Braun, D. Ewins, and S. Rao, eds., *Encyclopedia of Vibration*, Academic Press, pp. 673–685.
17. Kopsaftopoulos, F. P. 2012. *Advanced Functional and Sequential Statistical Time Series Methods for Damage Diagnosis in Mechanical Structures*, Ph.D. thesis, Department of Mechanical Engineering & Aeronautics, University of Patras, Patras, Greece.